

Arresting Photodegradation in Semiconducting Single-Walled Carbon Nanotube Thin Films

Bryon W. Larson, Kira A. Thurman, Hyun Suk Kang, Andrew J. Ferguson, Jeffrey L. Blackburn, and Mark Steger*



Cite This: *ACS Appl. Nano Mater.* 2022, 5, 3502–3511



Read Online

ACCESS |

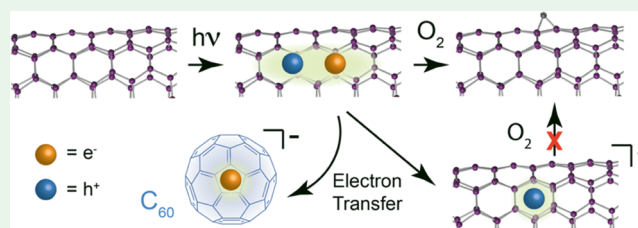
Metrics & More

Article Recommendations

Supporting Information

ABSTRACT: Solid-state dispersions of isolated single-walled carbon nanotubes (SWCNTs) in polymer matrices or networks of electronically coupled SWCNTs are gaining interest for a broad variety of optoelectronic applications. However, little is known about either the stability or degradation mechanisms of these systems. We show dramatic sp^2 -to- sp^3 defect transformations of the SWCNT sidewall when either the S_{11} or S_{22} exciton transitions are optically pumped in ambient conditions, leading to the rapid decay of absorption and emission properties in less than 24 h for conditions similar to exposure to solar illumination. Importantly, we demonstrate that either (i) encapsulation to block reactive O_2 from SWCNT excited states or (ii) exciton quenching via donor-to-acceptor electron transfer is an effective route for “kinetic stabilization” against photodegradation, with <8% loss in absorbance after 1200 h of illumination. We find that SWCNT:polymer loading does not impact degradation. Our study suggests that the sp^3 defects are associated with the formation of oxygenic groups on the SWCNT sidewall. While such defect populations can detrimentally evolve over time in films where SWCNTs are environmentally exposed in the presence of light, we offer multiple pathways to arrest this degradation and enable their robust application as advanced optical materials in optical and electronic devices.

KEYWORDS: carbon nanotubes, photodegradation, encapsulation, kinetic stabilization, photochemistry



INTRODUCTION

Now, 30 years since their discovery, single-walled carbon nanotubes (SWCNTs) have steadily advanced from a novel form of nanocarbon to a technologically relevant material with applications that range from photovoltaics^{1,2} to medicine³ to telecommunications.⁴ Much like their allotropic relatives—fullerenes—a major reason that SWCNTs exhibit such versatile functionalities is because their properties are highly tunable through both physical (i.e., tube size and chirality selection, endohedral filling, strategic formation of heterojunctions) and chemical routes (i.e., covalent modification of the nanotube sidewall with number, site, and adduct specificity).

Applications such as quantum emission⁵ and biological imaging⁶ can benefit from the tunable emission wavelength and enhanced quantum yield that result from the introduction of sp^3 sidewall defects with a high degree of specificity and design intention. Such advanced optoelectronic applications of SWCNTs require exquisite control when it comes to defect type, number, and location on the tubes, with most studies aimed at understanding the chemical routes to, and properties of, functionalized SWCNTs. In contrast, sp^3 sidewall defects are undesirable in applications such as transistors and photovoltaics, where the defect sites may serve as traps and recombination centers for charge carriers or excitons.⁷

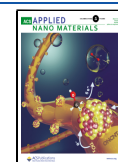
Consequently, for any potential technology, it is crucial to develop a fundamental understanding of how to maintain the chemical integrity of such sophisticatedly tailored or purified systems to ensure robust and consistent operation.

To date, studies of the stability or degradation of SWCNTs under real-world operating conditions have been limited. Consequently, the impacts of experimental and environmental conditions on the temporal evolution of defect populations (via optoelectronic properties) are still poorly understood. Over the last decade or so, there have been studies of the radiation hardness of carbon nanotube transistors and electronic circuits, in the context of extraterrestrial exposure to high energy radiation, which point to resistance of the carbon nanotube networks to chemical damage, due to the robustness of the C–C bonds to protons⁸ or γ rays.^{9–12} Similarly, the prevailing opinion in the community is that CNTs are inherently photostable when photoexcited in the visible and near-IR.^{13,14} As such, when degradation of devices

Received: December 2, 2021

Accepted: February 10, 2022

Published: February 28, 2022



is observed, it has generally been attributed to other constituents in the device.^{15,16} As an example, “photo-bleaching” of SWCNT emission intensity was observed for *s*-SWCNTs where O-related defects were created by ozonolysis, but the authors speculated that the photodegradation of surfactant micelles led to the creation of new exciton quenching sites.¹⁶ Flavel and Chen found recently that SWCNT/Nafion composite contacts enable high-efficiency silicon solar cells, but with poor long-term stability that the authors attributed to the hygroscopic nature of Nafion.¹⁵ Importantly, neither of these studies employed spectroscopic measurements that could report directly on the integrity of SWCNT sp^2 bonds (e.g., absorbance and/or Raman) to determine if the SWCNTs also experienced photodegradation.

In this work, we investigate the effects of the two most likely ambient stressors to SWCNTs (air and light) by monitoring singlet exciton absorption, emission, and corresponding Raman signature changes under continuous photodosing. Specifically, we show how quickly these ambient stressors can lead to SWCNT sidewall transformations that degrade the nanotubes’ optoelectronic properties. Yet, by elucidating factors that determine the decomposition pathway, we also show multiple effective strategies to arrest decomposition almost entirely. We focus this stability investigation on solid-state films of semiconducting (*s*-) SWCNTs, where the poly[(9,9-dioctyl-fluorenyl-2,7-diyl)-*alt-co*-(6,6’-(2,2’-bipyridine))] (PFO-BPy) wrapping polymer is highly selective for species having (*n,m*) chiral indices of (6,5). This (6,5) *s*-SWCNT is a commonly studied system that is currently being evaluated for a variety of novel applications.^{17–19} Our sample preparations cover a broad range of nanotube and polymer ratios in the solid state to model applications where the SWCNTs (i) may not be physically coupled (narrow band emitters), (ii) are almost entirely coupled (transport layers), and (iii) form an electron-transfer heterojunction with an acceptor (energy harvesting). We also account for different light stressors and excited-state degradation processes by selectively filtering the photobleaching lamp array to include or exclude photon absorption by the polymer and to also selectively photo-excite the nanotube’s lowest energy excitons.

We observe ambient light-induced oxidative degradation for (6,5) *s*-SWCNT:PFO-BPy systems, regardless of the extent of nanotube coupling or light filtering, with Raman and PL measurements showing changes that are consistent with the light-induced (excited-state) formation of sp^3 defects (Figure 1). Importantly, we demonstrate that dielectric encapsulation can almost entirely mitigate this degradation; continuous bleaching dynamics improve from fully bleached within a few days to only 3% bleached after more than 50 days. Our observations suggest that photoexcited *s*-SWCNTs can undergo light-induced degradation under ambient conditions and that exposure to highly reactive ozone or radicals (e.g., diazonium salts, azides, etc.) is not a prerequisite to rehybridizing their sp^2 bonds to form sp^3 defects.^{5,20} As an alternative to dielectric encapsulation, we also show that the photoreactive (6,5) *s*-SWCNT excited states can be kinetically stabilized in ambient conditions when an efficient and rapid electron-accepting species (e.g., C_{60}) is present, such as might be found in an *s*-SWCNT heterojunction-based photovoltaic device. These findings underscore that photodegradation processes during operation must be considered when designing and constructing optoelectronic devices containing *s*-SWCNTs with tailored optical and electronic properties. More

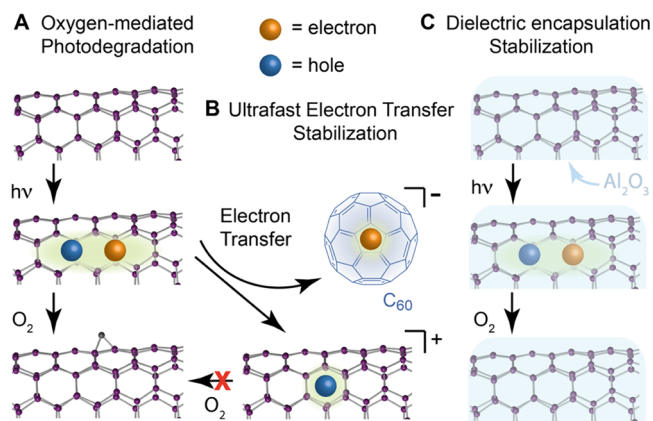


Figure 1. Scheme depicting (A) the observed photodegradation (via sp^3 oxygenic sidewall functionalization) of (6,5) *s*-SWCNT thin films. This photodegradation can be mitigated by (B) ultrafast electron transfer to a C_{60} acceptor or (C) dielectric encapsulation with Al_2O_3 .

importantly, we demonstrate that multiple options are available to ensure the robust operation of SWCNT-based optoelectronics, suggesting that such technologies are indeed a viable endeavor from the standpoint of intrinsic stability.

RESULTS AND DISCUSSION

To establish baseline photodegradation behaviors in air, we first discuss the ambient photobleaching dynamics of neat PFO-BPy films and films with (6,5) *s*-SWCNTs dispersed as isolated nanotubes within the polymer matrix. Continuous photodosing experiments were carried out on a custom-automated in situ photobleaching spectrometer (AIPS), as described previously²¹ and in the Supporting Information (SI) (Figure S1). Both polymer and (6,5) *s*-SWCNTs contribute to photon absorption in composite films since PFO-BPy absorbs wavelengths shorter than 400 nm and (6,5) *s*-SWCNTs have first (S_{11}) and second (S_{22}) excitonic absorbances at ~ 1000 and ~ 575 nm, respectively. We isolate the contributions of individual species to photodegradation by cross-examining photodosing experiments on a matrix of neat polymer and CNT-composite films using full spectrum as well as spectrally filtered irradiance conditions (using a 470 nm long-pass, LP, filter; see Figure S1) compiled in Figure 2.

Figure 2A,B compares bleaching behaviors between neat polymer and the (6,5) *s*-SWCNT composite by tracking the absorbance (FA) spectra over ca. 120 h of continuous irradiation. The AIPS data in Figure 2A demonstrate that the neat polymer absorbance (peak at 360 nm) degrades substantially during continuous unfiltered photodosing in air. It should be noted that the (6,5) *s*-SWCNTs studied in this paper exhibit a weak third (S_{33}) excitonic transition at ~ 350 nm as well. For the low SWCNT loadings we study, this absorption is negligible compared to that in the polymer (e.g., see SI part 6). When the composite film is subjected to the same unfiltered bleaching conditions (Figure 2B), the PFO-BPy still bleaches significantly but at a slightly slower rate relative to the neat film. From the normalized FA kinetics at 360 nm (Figure 2E, unfiltered), bleaching of the polymer absorbance is indeed marginally accelerated in the absence of the nanotubes, consistent with reports that related polymer systems can be stabilized against photodegradation through the addition of nanotubes.²² This slower bleaching of polymers in composite films can be understood in terms of PFO-BPy

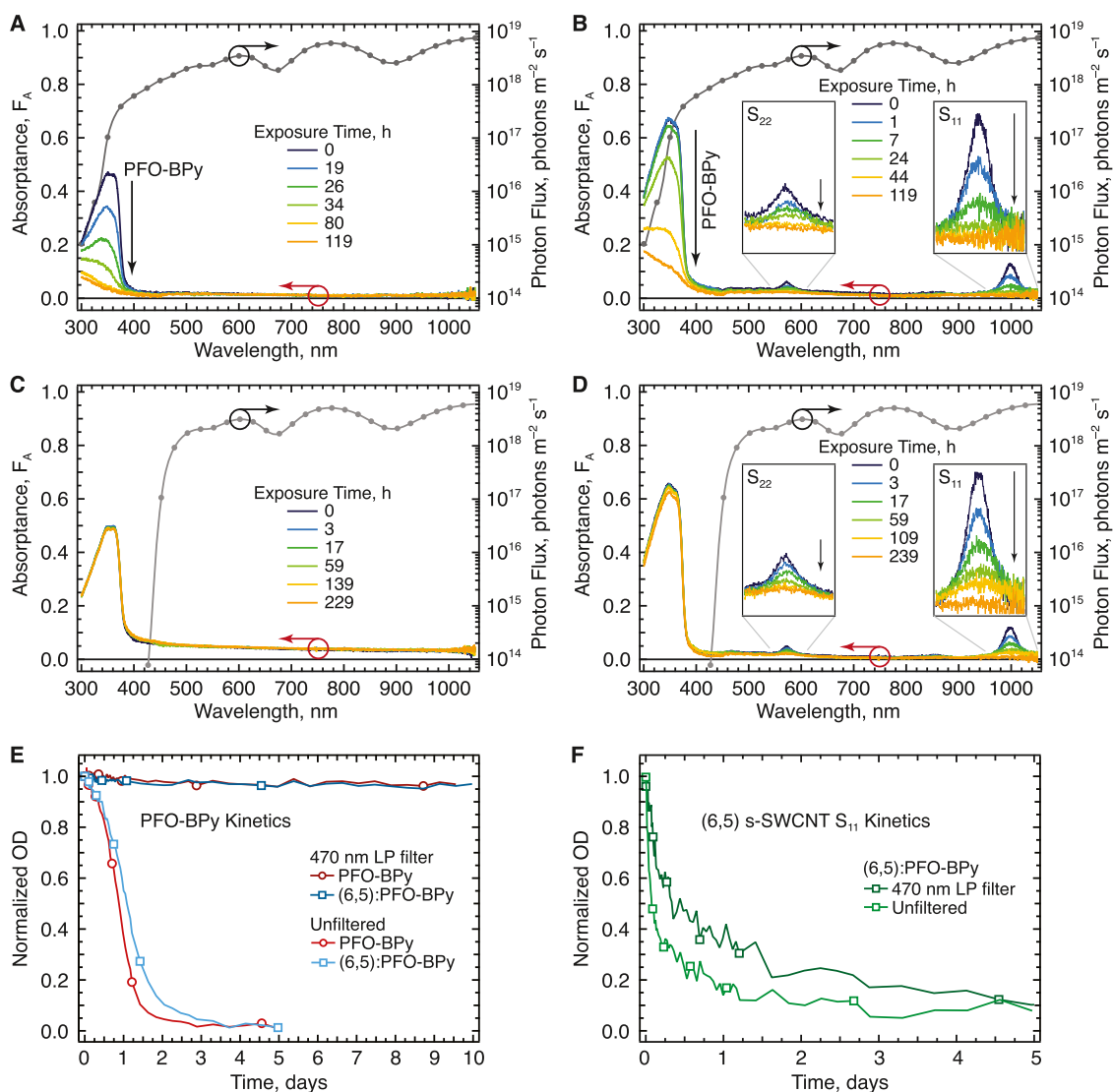


Figure 2. Panels (A–D): AIPS time-dependent FA spectra (left axes) and photobleaching irradiance spectral photon fluence (right axes) for a neat PFO-BPy film (panel A, unfiltered irradiation), a composite (6,5) s-SWCNT:PFO-BPy film (panel B, unfiltered irradiation), a neat PFO-BPy film (panel C, 470 nm filtered irradiation), and a composite (6,5) s-SWCNT:PFO-BPy film (panel D, 470 nm filtered irradiation). Arrows indicate the loss of polymer and (6,5) s-SWCNT absorbance features during the photobleaching experiment. Panels (E) and (F) show normalized time slices of optical density (OD) at 360 nm (tracking PFO-BPy) and 1000 nm (tracking the S_{11} exciton), respectively, for samples that were photobleached with and without filtering the irradiance spectrum using a 470 nm long-pass (LP) filter.

excitation energy transfer to the nanotubes.²³ Even so, we find that the PFO-BPy absorption only becomes steadfast when the photodosing array is filtered to avoid direct photoexcitation of the polymer (with a 470 nm LP filter), as shown in Figure 2C,D for the neat polymer and composite films, respectively. The time slices at 360 nm are also shown in Figure 2E (LP470-filtered, pure PFO-BPy) for reference to the unfiltered bleaching data, exhibiting only a 1.3% decrease over 240 h (10 days) of irradiation in air.

Turning to the bleaching behavior of the S_{11} and S_{22} optical transitions of the (6,5) s-SWCNTs, Figure 2B,D shows that either irradiance condition (unfiltered and 470 nm LP-filtered) results in the total loss of both nanotube exciton features in less than 100 h. Interestingly, when comparing the time-slice FA data at 1000 nm for the LP470-filtered vs unfiltered conditions (Figure 2F), the 1000 nm bleach dynamics do not appear to be strongly affected by the photoexcitation (or lack thereof) of the PFO-BPy host. This convincing result leads us to believe that

the decomposition mechanism affecting the polymer is self-contained. In other words, we see no significant evidence that the polymer degradation drastically alters the nanotube photobleach; degradation of the polymer is primarily commensurate with excitations on the polymer alone. We highlight the importance of this preliminary conclusion, as it suggests that using different wrapping polymers could be a path toward fine-tuning the stabilization of the polymer component and by extension the nanotube composite material. Of note, all of the spectral transformations discussed above appeared permanent. No recovery of the S_{11} or S_{22} exciton peaks was observed after storing the irradiated films in the dark in nitrogen, a preliminary indication that reversible photo-induced doping (i.e., reversible photoredox chemistry) or simple physisorption processes (vide infra) are not the dominant pathways for the loss of optical resonances.

Given the above observations, we sought to better understand their origins. The progressive, and eventually

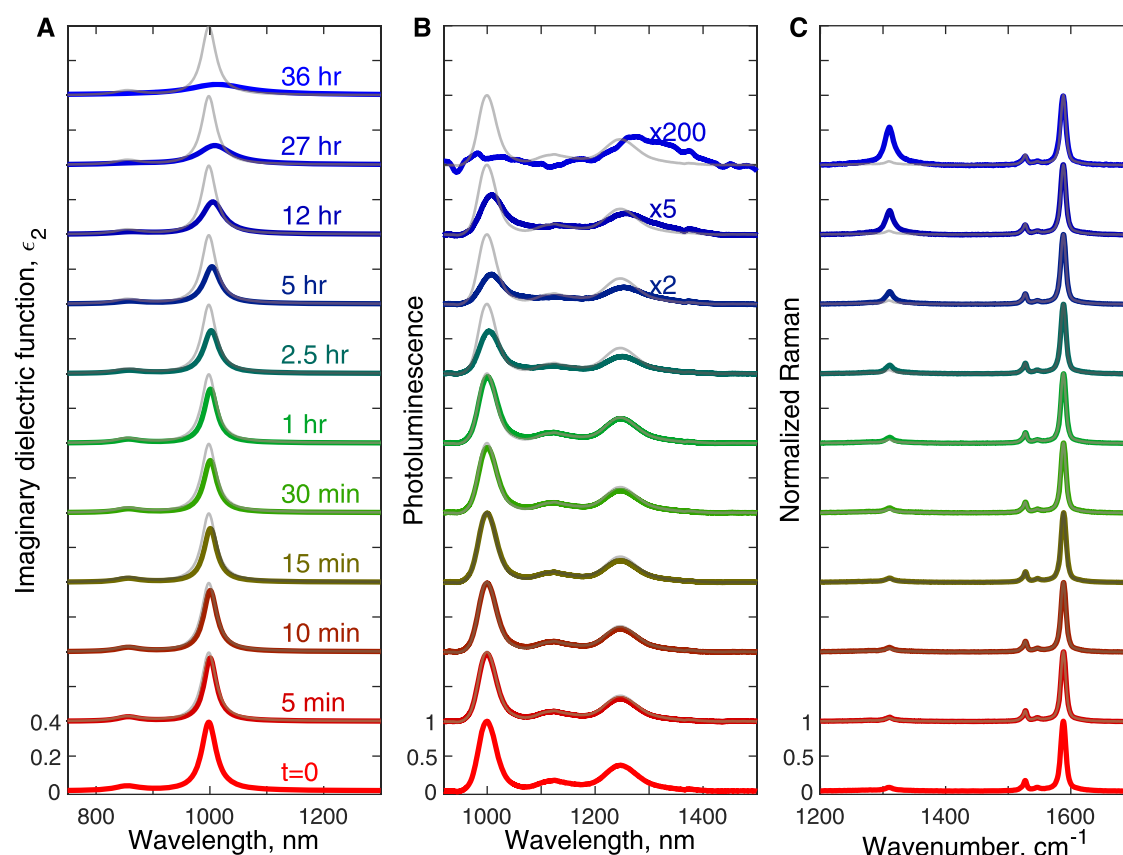


Figure 3. Spectroscopic characterization of degraded film evolution from pristine ($t = 0$) to significantly degraded (36 h exposure). Panel A: ellipsometry analysis of the oscillator strength changes in the S_{11} band and region of interest. Panel B: NIR PL emission, scaled to the initial oxide-encapsulated ($t = 0$) sample S_{11} emission peak. Panel C: Raman spectra, normalized to the signature sp^2 G-band. In each frame, the $t = 0$ spectrum is plotted in gray as a comparison to all other spectra.

complete, loss of S_{11} and S_{22} peak intensities suggests a corresponding loss of the sp^2 -hybridized orbitals and associated $\pi \rightarrow \pi^*$ transitions that provide oscillator strength to these optical resonances. We envisioned two most plausible explanations: (1) photodoping, potentially induced by light-assisted physisorption of molecules (e.g., oxygen, water) that can undergo redox chemistry with the SWCNTs or light-assisted charge transfer to/from physisorbed molecules, or (2) light-induced covalent bond formation with atmospheric molecules that convert nanotube sidewall sp^2 bonds to sp^3 bonds.

With these possible mechanisms in mind, we designed a systematic spectroscopic study to isolate, characterize, and track the degradation process over time. We subjected 10 identical (6,5) *s*-SWCNT:PFO-BPy films to up to 36 h of continuous ambient photobleaching (unfiltered light) and characterized the evolution of Raman scattering, near-infrared photoluminescence (NIR PL) emission intensity, and absorbance features of each film; the films were removed one at a time for full *ex situ* characterization. To prevent any obfuscation of the results by additional ambient exposure, each film was encapsulated with 100 nm alumina (demonstrated below to halt photodegradation) when removed from the bleaching apparatus to ensure no further degradation prior to (and/or during) optical characterization since our spectroscopies were conducted in air. (We found that direct, monochromatic injection into S_{22} caused rapid and continuous loss of S_{11} PL yield without encapsulation, similar to that observed on the AIPS.) The UV–vis–NIR spectra for all 10

films are shown in Figure S2, taken after removal from the bleaching setup and subsequent encapsulation. We note that the e-beam deposition process used to encapsulate each film has been shown to create a small population of emissive sp^3 defects, discussed more below. However, based on these reports,¹⁶ we estimate that the defect population generated by our encapsulation process would at most correspond to about 1/2 h of light exposure on the AIPS setup, meaning for the data shown in Figure 3 (36 h of light exposure), the observed kinetics are dominated by ambient photobleaching rather than any potential e-beam encapsulation effects.

As summarized in Figure 3, and discussed more below, we observe significant changes to the dielectric function, NIR PL, and Raman spectra (panels A–C, respectively) that are consistent with the continual growth of the sp^3 defect density on the SWCNT sidewalls. Of note, the ellipsometry data (see the full model in Figure S3) in Figure 3A immediately eliminate the photodoping hypothesis (1) mentioned above since no trace of the trion optical transition, a key indicator of a charge carrier population,²⁴ appears during illumination. To further confirm this, Figure S2 shows (for reference) the trion signature at ca. 1170 nm (a wavelength not accessible to our AIPS system) for (6,5) *s*-SWCNTs that were subjected to intentional chemical doping.²⁴ The complete, anisotropic dielectric function model for the films is presented in Figure S3. Accurately modeling the films this way removes artifacts due to thin film effects, film-to-film thickness variations, and evolution of the background refractive index due to the bleaching polymer. This ellipsometry analysis is sensitive to the

continuous bleaching, broadening, and red-shifting of the S_{11} mode, even while the PL and Raman show little change at early times and give no signal at the latest times.

The lack of a trion optical transition in the photodosed (6,5) films suggests that the S_{11} broadening and bleaching arise from another source, such as sidewall functionalization. Since sp^3 sidewall defects are known to form a bright and energetically distinct emission from localized sp^3 sites on the SWCNT,^{25,26} we turn to near-infrared (NIR) PL measurements to track such defect-related emission features. The PL spectra plotted in Figure 3B are scaled to the S_{11} emission counts at 1000 nm of the pristine film. As previously observed, we find that oxide encapsulation leads to relatively intense peaks at ca. 1130 and 1250 nm even at $t = 0$ (no photodosing), which have been attributed to oxygen-related defect sites induced by the oxide deposition step.¹⁶ Photodosing leads to a relative growth of defect PL emission between 1200 and 1500 nm, with a continual drop in S_{11} emission. Figure S4 more clearly shows the overall drop in the total PL intensity measured over a constant excitation power and detector integration time. No signal was detectable for the final film (36 h).

Semiempirical and density functional theory (DFT) calculations suggest that the most stable oxygenated SWCNT defects are epoxide and ether groups.^{20,27,28} The DFT studies of Ma et al. suggest that the lowest-energy emission peaks, with separations of ca. 135 and 310 meV from the S_{11} exciton emission, correspond to excitons strongly localized at “ether-d” (C–O–C bonds perpendicular to SWCNT axis) and “epoxide-I” (C–O–C bonds parallel to SWCNT axis) defect sites, respectively.²⁷ The same group showed that oxide thin film deposition onto (6,5) SWCNTs produced emission peaks corresponding to both ether-d and epoxide-I defect sites at room temperature.¹⁶ As such, we conclude that the PL peaks observed in Figure 3B at ca. 1130 and 1250 nm for both oxide-encapsulated and oxygen-modified (6,5) s-SWCNTs likely correspond to ether-d and epoxide-I defect groups, respectively.

The Raman spectral data over time (Figure 3C) also show classic behavior indicating sp^2 -to- sp^3 rehybridization,^{25,29} as evidenced by the growth of the D-band (ca. 1320 cm^{-1}) relative to the G-band (ca. 1592 cm^{-1}). The Raman spectra are normalized to the G-band intensity, and we see no change in the relative intensities of the sub-bands that comprise the G-band, even for the sample illuminated for 27 h. (We were unable to detect the G-band signal for the 36 h sample.) Since the D/G ratio is known to increase with the number density of sp^3 sidewall defects,²⁵ the continual growth of D/G during illumination suggests that the ambient photobleaching observed in the absorbance (Figure 2) is correlated with a continual sp^2 -to- sp^3 rehybridization. These results support the mechanism in hypothesis (2), whereby oxidative photodegradation occurs via the conversion of sp^2 bonds to oxygenic sp^3 sidewall defects, a possibility that has also been observed for a number of intentional oxygenic functionalization studies.^{16,20,27,30,31} Furthermore, and consistent with the ellipsometry results, no evidence of photodoping is observed, which is known to either change the scattering cross section or soften/stiffen the Raman modes, causing changes in the relative intensities or frequency shifts of the (6,5) s-SWCNT Raman bands.^{32,33}

From the thorough examination of the optical properties (Figure 3A–C), it is clear that a continuous and extensive conversion of sp^2 carbon to sp^3 occurs on the nanotubes

during ambient illumination, evidenced by (i) complete, irreversible loss of the nanotube S_{11} and S_{22} exciton peaks in the UV–vis–NIR absorption, (ii) a clear broadening of the S_{11} peak with no appearance of new absorption features in the IR spectrum that can be attributed to a trion for degraded films, (iii) growth of a red-shifted, deep defect PL band, and (iv) a gradual relative growth of the Raman scattering D-band.

With knowledge in hand regarding the photodegradation mechanism, we now turn our attention to strategies for arresting this degradation. Since photoinduced oxidative sp^3 defect formation is obviously thermodynamically spontaneous under ambient conditions, we explore routes for kinetic stabilization, whereby the rate of this spontaneous degradation pathway is either dramatically reduced or is outcompeted by another more desirable kinetic pathway. An obvious strategy for reducing the rate of oxygenic sidewall functionalization is to reduce or eliminate the access of oxygen to the photoexcited nanotubes. Thus, we utilized dielectric encapsulation on the film and repeated the AIPS testing in air. Figure 4

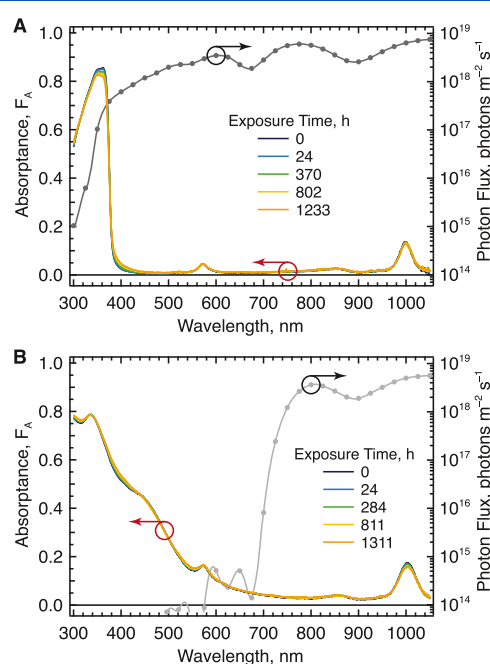


Figure 4. Illustrations of arresting photodegradation by (A) dielectric encapsulation of a (6,5) s-SWCNT:PFO-BPy film exposed to continuous unfiltered irradiation in air or (B) photoinduced electron transfer (PET) to a C_{60} electron acceptor in a (6,5) s-SWCNT:PFO-BPy/ C_{60} bilayer film exposed to continuous LP770-filtered irradiation in air.

demonstrates that, indeed, dielectric encapsulation with a thin (50–100 nm) coating of alumina confers >1200 h of photostability to both the PFO-BPy polymer and the (6,5) s-SWCNTs under unfiltered bleaching conditions.

We next examined whether an alternative pathway for the nanotube photoexcited state could provide effective kinetic competition to oxidative degradation. SWCNT-based photovoltaics operate on the principle broadly applied to “excitonic” solar cells, whereby bound electron–hole pairs (excitons) are rapidly dissociated at a donor/acceptor interface to produce “free” electrons in the acceptor phase and holes in the donor phase. (C_{60} -I_h)[5,6]fullerene (C_{60} , Buckminsterfullerene) has been utilized as a highly efficient electron acceptor for small-

diameter (6,5) and (7,5) s-SWCNTs³⁴ with exciton dissociation efficiencies as high as 85%³⁵ through rapid photoinduced electron transfer (PET) at the subpicosecond time scale.³⁶ As such, we hypothesized that the rapid removal of SWCNT electrons by photoinduced charge transfer to C₆₀ may prevent photodegradation in photovoltaic bilayers.

We prepared a bilayer of compact (6,5) s-SWCNTs with thermally evaporated C₆₀ on top and subjected the film to continuous ambient photodosing using a 770 nm long-pass (LP770)-filtered spectrum to ensure only the nanotube excited states were activated. As control experiments, we confirmed that the nanotube bleaching kinetics match the LP470 experiments (refer to Figure 2), where both the S₁₁ and the S₂₂ states were dosed in ambient, when no C₆₀ is present (see Figures S5 and S6). Figure 4b shows that when C₆₀ is present, the photodegradation pathway indeed appears to be out-competed by the rapid CT excited-state quenching pathway via electron transfer from the (6,5) s-SWCNT to C₆₀, evidenced by the steadfastness of the S₁₁ peak at 1000 nm, maintaining over 92% of the peak S₁₁ FA during the 1311 h long continuous irradiation experiment.

This result provides some insight into potential photodegradation mechanism(s), as depicted in Figure 5, although

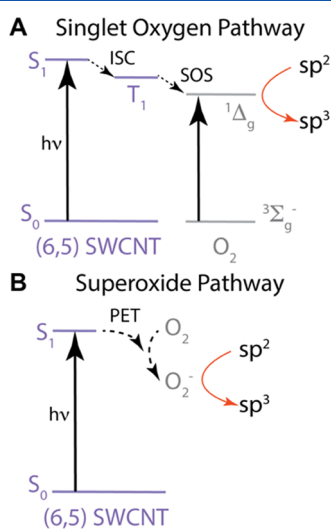


Figure 5. Potential pathways for the observed photodegradation. In both pathways, a photon ($h\nu$) first excites the SWCNT from the S₀ ground state to the first singlet excited-state S₁. (A) In the singlet oxygen pathway, intersystem crossing (ISC) converts some fraction of singlets to triplets (T₁), which can undergo singlet oxygen sensitization (SOS) via energy transfer that excites oxygen molecules from the ground triplet state to the excited singlet state. Reactive singlet oxygen molecules can react with the SWCNT sidewall to convert sp² to sp³ bonds. (B) In the superoxide pathway, photoinduced electron transfer (PET) occurs from either SWCNT excitons or SWCNT electrons that formed via autodissociation, converting oxygen molecules to superoxide molecules (O₂⁻). Reactive O₂⁻ molecules can react with the SWCNT sidewall to convert sp² to sp³ bonds.

some questions remain. Our prior studies demonstrate that the holes remaining in the SWCNTs following PET to C₆₀ are quite long-lived, lasting well beyond 5 ns,³⁶ a lifetime that is several orders of magnitude longer than the singlet exciton lifetime. Thus, we can be confident that excited-state holes alone are insufficient to drive the observed photodegradation. This leaves exciton- or electron-mediated pathways as potential

culprits for photodegradation. We speculate that one potential exciton-mediated process could be the intersystem crossing (ISC) of SWCNT singlet states to produce triplet excited states that are subsequently quenched by oxygen molecules (Figure 5A). Recent studies suggest that (6,5) s-SWCNT triplets are sufficiently energetic to sensitize singlet oxygen.³⁷ Long triplet lifetimes make this a prevalent reaction pathway for many organic molecules, and the highly reactive singlet oxygen molecules produced in such pathways are known to subsequently react with conjugated organic molecules.³⁸

Electron-driven radical formation and reaction, following resonant SWCNT excitation, have been proposed as a route for SWCNT sidewall functionalization with several different classes of molecules.^{5,39–41} In the current study, a potential one-electron pathway, involving only oxygen molecules (i.e., no protons), would be the reduction of oxygen molecules to generate superoxide radicals (Figure 5B).⁴² The redox potential of the O₂/O₂⁻ couple is -0.33 V vs the standard hydrogen electrode⁴³ or -4.11 V vs vacuum. This potential is roughly 250 mV more negative than the electron affinity (EA) value of -3.86 V vs vacuum proposed for (6,5) s-SWCNTs,⁴⁴ providing a thermodynamic driving force for this reaction. Interestingly, even though the SWCNT electron is transferred to C₆₀, there is no evidence for oxidation or dimerization of the C₆₀ cage in our spectral data (Figure S6), which would be a characteristic sharp peak around 428 nm, even after more than 1300 h of continuous photodosing. This implies that the energy lost during CT may be sufficient to avoid C₆₀ polymerization as well as photodegradation, which would be consistent with the EA value of ca. -4.29 V vs vacuum proposed for C₆₀,⁴⁵ making C₆₀ production of superoxide nonspontaneous. Future studies should explore the role of the acceptor's EA value, the rate of PET, and the lifetime of the charge-separated state on the effectiveness of this PET-based mechanism for mitigating photodegradation.

We note that we also compared a sample sealed in a “dry air” environment (0% relative humidity)⁴⁶ to a sample sealed in an “ambient air” environment (11–15% relative humidity) to probe the degree to which water molecules may impact the functionalization (e.g., through hydroxyl radical formation). We observed a negligible difference in the photodegradation kinetics of these two samples (Figure S7), indicating that water molecules are not required to drive the photodegradation. The potential role that water molecules, especially in higher humidity environments, may play in accelerating the photodegradation should be explored in future experiments.

Finally, since physically blocking the access of oxygen molecules to the SWCNT surfaces with Al₂O₃ dramatically reduces the rate of photodegradation, we also probed the degree to which the excess polymer host matrix may provide any physical barrier to SWCNT degradation. Figure 6 shows the S₁₁ degradation kinetics for several (6,5) s-SWCNT:PFO-BPy films with varying polymer content. These samples were either prepared by spin-coating (as for the high-polymer-content samples presented earlier in this study) or prepared by spray-coating (required to generate sufficiently thick samples with low polymer content for subsequent photodegradation and optical characterization). The latter samples, with the lowest polymer content, were prepared via centrifugation-based and post-deposition removal of excess PFO-BPy, ultimately down to a point where the film primarily exists as highly interconnected SWCNTs, with only the small amount of PFO-BPy remaining that is strongly wrapped around the s-

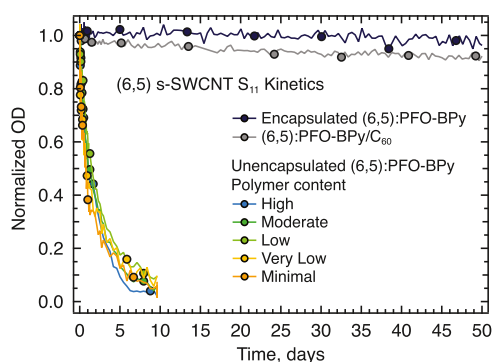


Figure 6. Comparison of bleaching rates of the time-dependent optical density (OD) data normalized to the $t = 0$ amplitude of the S_{11} absorbance peak (centered at 1000 nm) for a broad range of (6,5) s-SWCNT:PFO-BPy ratios, plotted against exposure time to illustrate the inefficacy of the polymer host at preventing oxygen access to the carbon nanotube surface, compared to a (6,5):PFO-BPy sample encapsulated by Al_2O_3 and a (6,5):PFO-BPy/ C_{60} bilayer.

SWCNTs. For all films, the S_{11} absorbance peak was tracked via the normalized OD at 1000 nm (Figure 6). For reference, the encapsulated film and C_{60} bilayer data are also shown, which showed minimal loss of the S_{11} feature for the experiment duration of over 1200 h. On the other hand, all of the unencapsulated films exhibited rapid loss of S_{11} peak absorbance. Interestingly, the irreversible rate of S_{11} photo-bleach appears to be somewhat independent of the relative amount of polymer in each film, judged by the ratio of the PFO-BPy peak at 360 nm relative to the S_{11} SWCNT peak (Figure S8). Figure 6 suggests that the PFO-BPy polymer matrix is substantially less effective at blocking oxygen ingress and reaction with the excited states on (6,5) SWCNTs than a thin oxide layer.

One should note that it is not terribly surprising that even a high loading of polymer is inadequate as an environmental barrier. Polymers, and especially light-emitting polymers,⁴⁷ are known to be highly permeable to gases such as O_2 . On the other hand, thin metal or metal-oxide layers can be excellent gas diffusion barriers, provided they are uniform and dense. Although e-beam-evaporated films can be noncontinuous, we constantly rotate the substrate during deposition from an off-center source to reduce the pore/crack density and maximize coverage. Even though atomic layer deposition (ALD) could potentially provide a more conformal coating than evaporation techniques, our data appear to show that our e-beam-evaporated oxide is sufficient to afford long-term protection of the underlying CNT film.

CONCLUSIONS

In this study, we investigated the photostability of technologically relevant blends of PFO-BPy and (6,5) s-SWCNTs under a variety of conditions and presented four key findings. First, the optoelectronic pumping of the SWCNT singlet exciton in air drives an irreversible bleach of these features, characterized by the loss of conjugation on the carbon nanotube as sp^2 carbons are photochemically converted to sp^3 . Second, these observations are reproduced regardless of whether the PFO-BPy polymer also participates in photon absorption and regardless of whether the tubes have high connectivity in the film or if they are dilutely dispersed within the host polymer matrix. Under these ambient conditions, the S_{11} exciton is

completely bleached within 6 days during continuous irradiation with ~ 1.1 sun equivalent of broad-band white light. Third, we find that the dielectric encapsulation of the blend films completely arrests these degradation pathways, which extends extrapolated lifetimes to longer than 100 years (essentially no degradation observed over more than 1200 h of continuous testing) in air. Finally, we find that the rapid extraction of photoexcited electrons from (6,5) s-SWCNTs in donor/acceptor bilayers kinetically outcompetes the photo-degradation mechanism. The results of this study provide important mechanistic insights into the potential degradation pathways of highly enriched s-SWCNTs as active layers in associated devices, along with concrete strategies toward mitigating such degradation for robustly operational SWCNT technologies for optoelectronic applications.

Ultimately, these results are specific to (6,5) s-SWCNTs photoexcited in air. Such nanotubes exhibit excellent stability in the absence of oxygen, which has likely contributed to the belief that they are generally photostable. We find that photoexcitation at either the S_{11} or S_{22} to form excitons is sufficient to drive this oxygen-related degradation. While we do not test for stability under electronic injection of carriers, it seems likely that any system, which forms excitons in the SWCNT component, will be at risk of this degradation, and this should be further studied. Lastly, we note that (6,5) tubes have a small diameter and therefore a higher π -orbital vector strain, which in fullerenes is known to increase carbon cage reactivity.⁴⁸ Similar studies may in fact show that larger diameter SWCNTs could be intrinsically more stable.

EXPERIMENTAL SECTION

Sample Preparation. A dispersion of 0.5 mg/mL of commercial (6,5)-enriched SWCNT powder (CHASM Inc.) was probe tip-sonicated with 2 mg/mL poly[(9,9-dioctylfluorenyl-2,7-diyl)-*alt*-co-(6,6'-{2,2'-bipyridine})] (PFO-BPy, American Dye Source, Inc., $M_w = 35\text{--}65$ kDa) in toluene (Analytical Grade; Fisher Scientific Inc.) using a 0.5 in. probe tip for 15 min at 300 W (Cole-Parmer CPX 750) in a flowing water bath at room temperature. All centrifuge runs were conducted using an SW32Ti swinging-bucket rotor and Beckman-Coulter Optima L100XP ultracentrifuge. The tip-sonicated samples were immediately centrifuged at 13 200 rpm (29 760g) for 5 min at 20 °C. The purple supernatant (ca. 15 mL) was recovered and concentrated to approximately 5 mL by heating to 80 °C on a hot plate and passing a gentle stream of nitrogen over the solution surface. Six concentrated samples were combined together and centrifuged at 24 100 rpm (99 202g) for 20 h at 20 °C, and the (6,5):PFO-BPy pellet was recovered using approximately 0.5 mL of supernatant. The solution was combined with other recovered pellet solutions, and the supernatant was added to reach the desired volume (1–3 mL). Inks used for spray-coating were prepared the same way but dispersed in 10–15 mL of neat toluene after final centrifugation.

For solutions that required a smaller volume of toluene than what was needed to recover the pellets, all pellets were dispersed together in 20–30 mL of supernatant and centrifuged at 24 100 rpm (99 202g) for 40 h at 20 °C. The resulting pellet was recovered using a thin spatula and dispersed in a desired amount of supernatant (1–3 mL). PFO-BPy powder was added until the ink reached the concentration to maintain the desired [(6,5)]:[PFO-BPy] ratio.

Thin films were prepared by spin-coating or spray-coating onto clean, polished quartz substrates (25 mm \times 11 mm \times 1 mm). To ensure a homogeneous dispersion, inks were bath-sonicated immediately before deposition. For spin-coated samples, thin films were prepared by applying 100 μ L of warm (~ 70 °C) SWCNT:PFO-BPy solution onto room-temperature quartz plates in a dry nitrogen atmosphere glovebox at 4000 rpm for blend solutions or 6000 rpm for neat PFO-BPy solutions using a 1 s ramp time and a 60 s total spin

time. All films were stored under dry nitrogen and protected from UV while not being used for measurements in air. Spray-coated samples were prepared by spraying dilute inks at 300 $\mu\text{L}/\text{min}$, directed by a stream of dry nitrogen gas at 7 std L/min, onto the quartz substrates on a heated stage ($130 \pm 10^\circ\text{C}$) using an ultrasonic spray head (SonoTek, 0.8 W), with raster pattern designed to maximize uniformity over the sample area. The films were left on the hot plate for several minutes after spraying to ensure they were completely dry. For the (6,5) SWCNT/ C_{60} donor/acceptor bilayer, ~ 90 nm of C_{60} was deposited on the SWCNT thin film via thermal evaporation at a pressure of $<1 \times 10^{-6}$ Torr and a deposition rate of 0.5 $\text{\AA}/\text{s}$.

UV-vis-NIR measurements were carried out on inks or thin film samples using either a Cary 5000 or 7000 spectrometer in dual beam transmission mode, with reference baselines taken either from toluene in a 2 mm cuvette for solution measurements or through a blank quartz substrate for film measurements, respectively.

Controlled Photon Dosing and Degradation. A custom-built automated in situ photobleaching spectrometer (AIPS) was used to record time-dependent photobleaching dynamics of the thin film samples. The same instrument has been described previously in detail.²¹ The system consists of a 4-bulb array (Sylvania 58321) that outputs ~ 1.11 sun equiv (~ 110 mW/cm^2) of photon flux between 300 and 1100 nm (refer to the right y-axis in Figures 1A,B and S1 in the Supporting Information) that is mounted above a rotating platter of samples. The time-dependent absorbance (fraction of absorbed light, FA) spectra are sampled in situ via dual spectrometers (transmittance and reflectance) during the course of the experiment.

In situ spectroscopic measurements are enabled by a separate light source (Ocean Optics DH-2000-BAL) and two spectrometers (Ocean Optics HR2000 and Ocean Optics R400-7-SR). The incident light is guided to the sample through the core of a “six around one” reflectance probe, where the six external fibers collect the reflected light. A collimating lens is used to capture the transmitted light into a single core fiber. These separate reflectance (FR) and transmittance (FT) measurements are used to determine the fraction of absorbed light, which is calculated by $\text{FA} = 1 - \text{FR} - \text{FT}$. The measurements were carried out in air, and the temperature of the sample platter was monitored during the experiment. Glass long-pass or laminated notch filters were used to tune the bulb array output spectrum (transmission profiles of the filters and the corresponding spectral photon fluence spectra are shown in Figure S1). The photon intensity of the bulb array in this experiment was measured as 2.2×10^{17} photons/(s m^2) at 360 nm, the peak absorbance wavelength of the polymer, for the unfiltered irradiance conditions and calculated as $<5 \times 10^{13}$ photons/(s m^2) at the same wavelength with the LP470 filter in place. It should be noted that the absorbance spectra have not been corrected for contributions to the measured spectrum from the quartz substrate (cf., the feature between 450 and 500 nm) supporting each film.

Photoluminescence, Raman, and Ellipsometric Spectroscopy Measurements. Infrared photoluminescence excitation using a home-built PL instrument⁴⁹ was used to confirm that our films are highly monochiral. A separate Princeton PL spectrometer system was used to measure S_{11} PL yield while directly exciting the S_{22} transition at (574 nm) and recorded on an InGaAs array (full details in SI part 4). Raman spectra were excited resonant to the S_{22} in a backscattering configuration and recorded using a Jobin Yvon T64000 triple spectrometer with a nitrogen-cooled silicon charge-coupled device (CCD). Multimodal ellipsometry combines transmission-absorbance data with reflection and transmission spectroscopic ellipsometry to model the dielectric function of encapsulated films (full methods in SI part 3).

Thin Film Encapsulation. Encapsulation was achieved by the e-beam deposition of alumina coatings around 50–100 nm thick. The substrate was rotated during the deposition and maintained at roughly a 30° angle with respect to the line of sight to the target. It is possible that the deposition thickness, rotation, and slight oblique angle aid in the effectiveness of the e-beam film, which likely exhibits some scale of porosity. To minimize exposure of the films, we run the deposition at room temperature and do not flow any oxygen or plasma. For NIR PL, Raman, and NIR absorption spectral characterization of degraded

films, we encapsulate the films after photon dosing on the AIPS to prevent further photodegradation. However, we recognize that the e-beam deposition of dielectrics has the potential to slightly oxidize the tubes during the first 10 nm or so of the deposition, and therefore, we account for this in the analysis and find that it does not impact the overall degradation kinetics observed.

■ ASSOCIATED CONTENT

Supporting Information

The Supporting Information is available free of charge at <https://pubs.acs.org/doi/10.1021/acsnm.1c04140>.

Details on AIPS method; ruling out trion signature; ellipsometry methods; PL methods; kinetics of defect formation; evolution of heterojunction absorption; probing the impact of ambient humidity; and quantifying SWCNT concentration across samples (PDF)

■ AUTHOR INFORMATION

Corresponding Author

Mark Steger – National Renewable Energy Laboratory, Golden, Colorado 80401, United States; orcid.org/0000-0002-5907-2493; Email: mds71@pitt.edu

Authors

Bryon W. Larson – National Renewable Energy Laboratory, Golden, Colorado 80401, United States; orcid.org/0000-0002-0934-987X

Kira A. Thurman – National Renewable Energy Laboratory, Golden, Colorado 80401, United States

Hyun Suk Kang – National Renewable Energy Laboratory, Golden, Colorado 80401, United States

Andrew J. Ferguson – National Renewable Energy Laboratory, Golden, Colorado 80401, United States; orcid.org/0000-0003-2544-1753

Jeffrey L. Blackburn – National Renewable Energy Laboratory, Golden, Colorado 80401, United States; orcid.org/0000-0002-9237-5891

Complete contact information is available at: <https://pubs.acs.org/doi/10.1021/acsnm.1c04140>

Notes

The authors declare no competing financial interest.

■ ACKNOWLEDGMENTS

This work was authored by the National Renewable Energy Laboratory, operated by Alliance for Sustainable Energy, LLC, for the U.S. Department of Energy (DOE) under Contract No. DE-AC36-08GO28308. This work was supported by the Laboratory Directed Research and Development (LDRD) Program at NREL. Work exploring the role of photoinduced charge transfer on mitigating photodegradation was supported by the Solar Photochemistry Program, Division of Chemical Sciences, Geosciences, and Biosciences, Office of Basic Energy Sciences, U.S. Department of Energy (DOE). The views expressed in the article do not necessarily represent the views of the DOE or the U.S. Government. The U.S. Government retains and the publisher, by accepting the article for publication, acknowledges that the U.S. Government retains a nonexclusive, paid-up, irrevocable, worldwide license to publish or reproduce the published form of this work, or allow others to do so, for U.S. Government purposes. M.S. thanks Nina Hong and James Hilficker of J. A. Woollam for advice on optical modeling.

REFERENCES

- (1) Blackburn, J. L. Semiconducting Single-Walled Carbon Nanotubes in Solar Energy Harvesting. *ACS Energy Lett.* **2017**, *2*, 1598–1613.
- (2) Habisreutinger, S. N.; Blackburn, J. L. Carbon Nanotubes in High-Performance Perovskite Photovoltaics and Other Emerging Optoelectronic Applications. *J. Appl. Phys.* **2021**, *129*, No. 010903.
- (3) Deshmukh, M. A.; Jeon, J.-Y.; Ha, T.-J. Carbon Nanotubes: an Effective Platform for Biomedical Electronics. *Biosens. Bioelectron.* **2020**, *150*, No. 111919.
- (4) He, X.; Hartmann, N. F.; Ma, X.; Kim, Y.; Ihly, R.; Blackburn, J. L.; Gao, W.; Kono, J.; Yomogida, Y.; Hirano, A.; Tanaka, T.; Kataura, H.; Htoon, H.; Doorn, S. K. Tunable Room-Temperature Single-Photon Emission at Telecom Wavelengths From Sp 3 Defects in Carbon Nanotubes. *Nat. Photonics* **2017**, *11*, 577–582.
- (5) Brozena, A. H.; Kim, M.; Powell, L. R.; Wang, Y. H. Controlling the Optical Properties of Carbon Nanotubes with Organic Colour-Centre Quantum Defects. *Nat. Rev. Chem.* **2019**, *3*, 375–392.
- (6) Diao, S.; Blackburn, J. L.; Hong, G.; Antaris, A. L.; Chang, J.; Wu, J. Z.; Zhang, B.; Cheng, K.; Kuo, C. J.; Dai, H. Fluorescence Imaging in Vivo at Wavelengths Beyond 1500 Nm. *Angew. Chem.* **2015**, *14758*–14762.
- (7) Wang, J.; Shea, M. J.; Flach, J. T.; McDonough, T. J.; Way, A. J.; Zanni, M. T.; Arnold, M. S. Role of Defects as Exciton Quenching Sites in Carbon Nanotube Photovoltaics. *J. Phys. Chem. C* **2017**, *121*, 8310–8318.
- (8) Hong, W. K.; Lee, C.; Nepal, D.; Geckeler, K. E.; Shin, K.; Lee, T. Radiation Hardness of the Electrical Properties of Carbon Nanotube Network Field Effect Transistors Under High-Energy Proton Irradiation. *Nanotechnology* **2006**, *17*, 5675–5680.
- (9) Zhu, M.; Zhou, J.; Sun, P.; Peng, L.-M.; Zhang, Z. Analyzing Gamma-Ray Irradiation Effects on Carbon Nanotube Top-Gated Field-Effect Transistors. *ACS Appl. Mater. Interfaces* **2021**, *13*, 47756–47763.
- (10) Zhu, M. G.; Zhang, Z.; Peng, L.-M. High-Performance and Radiation-Hard Carbon Nanotube Complementary Static Random-Access Memory. *Adv. Electron. Mater.* **2019**, *5*, No. 1900313.
- (11) Zhu, M.; Xiao, H.; Yan, G.; Sun, P.; Jiang, J.; Cui, Z.; Zhao, J.; Zhang, Z.; Peng, L.-M. Radiation-Hardened and Repairable Integrated Circuits Based on Carbon Nanotube Transistors with Ion Gel Gates. *Nat. Electron.* **2020**, *3*, 622–629.
- (12) McMorrow, J. J.; Cress, C. D.; Gaviria Rojas, W. A.; Geier, M. L.; Marks, T. J.; Hersam, M. C. Radiation-Hard Complementary Integrated Circuits Based on Semiconducting Single-Walled Carbon Nanotubes. *ACS Nano* **2017**, *11*, 2992–3000.
- (13) Hong, G.; Diao, S.; Antaris, A. L.; Dai, H. Carbon Nanomaterials for Biological Imaging and Nanomedical Therapy. *Chem. Rev.* **2015**, *115*, 10816–10906.
- (14) Graf, A.; Tropf, L.; Zakharko, Y.; Zaumseil, J.; Gather, M. C. Near-Infrared Exciton-Polaritons in Strongly Coupled Single-Walled Carbon Nanotube Microcavities. *Nat. Commun.* **2016**, *7*, No. 13078.
- (15) Yan, J.; Zhang, C.; Li, H.; Yang, X.; Wan, L.; Li, F.; Qiu, K.; Guo, J.; Duan, W.; Lambert, A.; Lu, W.; Song, D.; Ding, K.; Flavel, B. S.; Chen, J. Stable Organic Passivated Carbon Nanotube–Silicon Solar Cells with an Efficiency of 22%. *Adv. Sci.* **2021**, *8*, No. e2102027.
- (16) Ma, X.; Baldwin, J. K. S.; Hartmann, N. F.; Doorn, S. K.; Htoon, H. Solid-State Approach for Fabrication of Photostable, Oxygen-Doped Carbon Nanotubes. *Adv. Funct. Mater.* **2015**, *25*, 6157–6164.
- (17) Zaumseil, J. Recent Developments and Novel Applications of Thin Film, Light-Emitting Transistors. *Adv. Funct. Mater.* **2020**, *30*, No. 1905269.
- (18) Rother, M.; Brohmann, M.; Yang, S.; Grimm, S. B.; Schießl, S. P.; Graf, A.; Zaumseil, J. Aerosol-Jet Printing of Polymer-Sorted (6,5) Carbon Nanotubes for Field-Effect Transistors with High Reproducibility. *Adv. Electron. Mater.* **2017**, *3*, No. 1700080.
- (19) Graf, A.; Murawski, C.; Zakharko, Y.; Zaumseil, J.; Gather, M. C. Infrared Organic Light-Emitting Diodes with Carbon Nanotube Emitters. *Adv. Mater.* **2018**, *30*, No. e1706711.
- (20) Ghosh, S.; Bachilo, S. M.; Simonette, R. A.; Beckingham, K. M.; Weisman, R. B. Oxygen Doping Modifies Near-Infrared Band Gaps in Fluorescent Single-Walled Carbon Nanotubes. *Science* **2010**, *330*, 1656–1659.
- (21) Garner, L. E.; Nellissery Viswanathan, V.; Arias, D. H.; Brook, C. P.; Christensen, S. T.; Ferguson, A. J.; Kopidakis, N.; Larson, B. W.; Owczarczyk, Z. R.; Pfeilsticker, J. R.; Ramamurthy, P. C.; Strauss, S. H.; Boltalina, O. V.; Braunecker, W. A. Photobleaching Dynamics in Small Molecule: vs. Polymer Organic Photovoltaic Blends with 1,7-Bis-Trifluoromethylfullerene. *J. Mater. Chem. A* **2018**, *6*, 4623–4628.
- (22) Luck, K. A.; Arnold, H. N.; Shastry, T. A.; Marks, T. J.; Hersam, M. C. Suppression of Polyfluorene Photo-Oxidative Degradation via Encapsulation of Single-Walled Carbon Nanotubes. *J. Phys. Chem. Lett.* **2016**, *7*, 4223–4229.
- (23) Balcı Leinen, M.; Berger, F. J.; Klein, P.; Mühlinghaus, M.; Zorn, N. F.; Settele, S.; Allard, S.; Scherf, U.; Zaumseil, J. Doping-Dependent Energy Transfer From Conjugated Polyelectrolytes to (6,5) Single-Walled Carbon Nanotubes. *J. Phys. Chem. C* **2019**, *123*, 22680–22689.
- (24) Ferguson, A. J.; Reid, O. G.; Nanayakkara, S. U.; Ihly, R.; Blackburn, J. L. Efficiency of Charge-Transfer Doping in Organic Semiconductors Probed with Quantitative Microwave and Direct-Current Conductance. *J. Phys. Chem. Lett.* **2018**, *9*, 6864–6870.
- (25) Piao, Y.; Meany, B.; Powell, L. R.; Valley, N.; Kwon, H.; Schatz, G. C.; Wang, Y. Brightening of Carbon Nanotube Photoluminescence Through the Incorporation of Sp 3 Defects. *Nat. Chem.* **2013**, *5*, 840–845.
- (26) Miyauchi, Y.; Iwamura, M.; Mouri, S.; Kawazoe, T.; Ohtsu, M.; Matsuda, K. Brightening of Excitons in Carbon Nanotubes on Dimensionality Modification. *Nat. Photonics* **2013**, *7*, 715–719.
- (27) Ma, X.; Adamska, L.; Yamaguchi, H.; Yalcin, S. E.; Tretiak, S.; Doorn, S. K.; Htoon, H. Electronic Structure and Chemical Nature of Oxygen Dopant States in Carbon Nanotubes. *ACS Nano* **2014**, *8*, 10782–10789.
- (28) Yim, W. L.; Karl Johnson, J. Ozone Oxidation of Single Walled Carbon Nanotubes From Density Functional Theory. *J. Phys. Chem. C* **2009**, *113*, 17636–17642.
- (29) Kalbacova, J.; Garratt, E.; Rodriguez, R. D.; Hight Walker, A. R.; Twedt, K. A.; Fagan, J. A.; Madeira, T. I.; McClelland, J. J.; Nikoobakht, B.; Zahn, D. R. T. Defect Evolution of Ion-Exposed Single-Wall Carbon Nanotubes. *J. Phys. Chem. C* **2019**, *123*, 2496–2505.
- (30) Ma, X.; Hartmann, N. F.; Baldwin, J. K. S.; Doorn, S. K.; Htoon, H. Room-Temperature Single-Photon Generation From Solitary Dopants of Carbon Nanotubes. *Nat. Nanotechnol.* **2015**, *10*, 671–675.
- (31) Iizumi, Y.; Yudasaka, M.; Kim, J.; Sakakita, H.; Takeuchi, T.; Okazaki, T. Oxygen-Doped Carbon Nanotubes for Near-Infrared Fluorescent Labels and Imaging Probes. *Sci. Rep.* **2018**, *8*, No. 6272.
- (32) Hao, J.; Nanayakkara, S. U.; Tervo, E. J.; Blackburn, J. L.; Ferguson, A. J. High-Performance Carbon Nanotube Electronic Ratchets. *Energy Environ. Sci.* **2021**, *14*, 5457–5468.
- (33) Suzuki, S.; Hibino, H. Characterization of Doped Single-Wall Carbon Nanotubes by Raman Spectroscopy. *Carbon* **2011**, *49*, 2264–2272.
- (34) Ferguson, A. J.; Dowgiallo, A.-M.; Bindl, D. J.; Mistry, K. S.; Reid, O. G.; Kopidakis, N.; Arnold, M. S.; Blackburn, J. L. Trap-Limited Carrier Recombination in Single-Walled Carbon Nanotube Heterojunctions with Fullerene Acceptor Layers. *Phys. Rev. B* **2015**, *91*, No. 245311.
- (35) Bindl, D. J.; Arnold, M. S. Efficient Exciton Relaxation and Charge Generation in Nearly Monochiral (7,5) Carbon Nanotube/C₆₀ Thin-Film Photovoltaics. *J. Phys. Chem. C* **2013**, *117*, 2390–2395.
- (36) Dowgiallo, A.-M.; Mistry, K. S.; Johnson, J. C.; Blackburn, J. L. Ultrafast Spectroscopic Signature of Charge Transfer Between Single-Walled Carbon Nanotubes and C₆₀. *ACS Nano* **2014**, *8*, 8573–8581.
- (37) Lin, C. W.; Bachilo, S. M.; Weisman, R. B. Delayed Fluorescence From Carbon Nanotubes Through Singlet Oxygen-

Sensitized Triplet Excitons. *J. Am. Chem. Soc.* **2020**, *142*, 21189–21196.

(38) Wilson, T. Excited Singlet Molecular Oxygen in Photo-oxidation. *J. Am. Chem. Soc.* **1966**, *88*, 2898–2902.

(39) Powell, L. R.; Piao, Y.; Wang, Y. Optical Excitation of Carbon Nanotubes Drives Localized Diazonium Reactions. *J. Phys. Chem. Lett.* **2016**, *7*, 3690–3694.

(40) Wu, X.; Kim, M.; Kwon, H.; Wang, Y. H. Photochemical Creation of Fluorescent Quantum Defects in Semiconducting Carbon Nanotube Hosts. *Angew. Chem., Int. Ed.* **2018**, *57*, 648–653.

(41) He, X.; Kevlishvili, I.; Murcek, K.; Liu, P.; Star, A. Photocycloaddition of Enones to Single-Walled Carbon Nanotubes Creates Fluorescent Quantum Defects. *ACS Nano* **2021**, *15*, 4833–4844.

(42) Hoke, E. T.; Sachs-Quintana, I. T.; Lloyd, M. T.; Kauvar, I.; Mateker, W. R.; Nardes, A. M.; Peters, C. H.; Kopidakis, N.; McGehee, M. D. The Role of Electron Affinity in Determining Whether Fullerenes Catalyze or Inhibit Photooxidation of Polymers for Solar Cells. *Adv. Energy Mater.* **2012**, *2*, 1351–1357.

(43) Krumova, K.; Cosa, G. *Overview of Reactive Oxygen Species; The Royal Society of Chemistry*, 2016; Vol. 1, pp 3–21.

(44) Kang, H. S.; Sisto, T. J.; Peurifoy, S.; Arias, D. H.; Zhang, B.; Nuckolls, C.; Blackburn, J. L. Long-Lived Charge Separation at Heterojunctions Between Semiconducting Single-Walled Carbon Nanotubes and Perylene Diimide Electron Acceptors. *J. Phys. Chem. C* **2018**, *122*, 14150–14161.

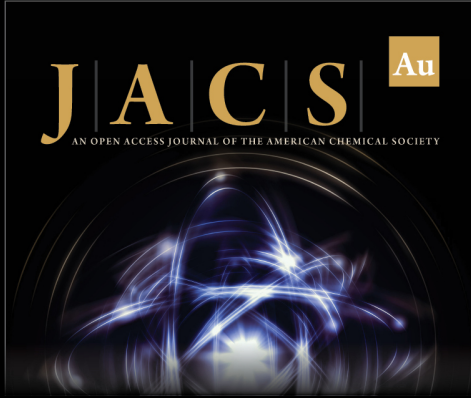
(45) Ihly, R.; Mistry, K. S.; Ferguson, A. J.; Clikeman, T. T.; Larson, B. W.; Reid, O.; Boltalina, O. V.; Strauss, S. H.; Rumbles, G.; Blackburn, J. L. Tuning the Driving Force for Exciton Dissociation in Single-Walled Carbon Nanotube Heterojunctions. *Nat. Chem.* **2016**, *8*, 603–609.

(46) Zhang, H.; Dunklin, J. R.; Reid, O. G.; Yun, S. J.; Nanayakkara, S. U.; Lee, Y. H.; Blackburn, J. L.; Miller, E. M. Disentangling Oxygen and Water Vapor Effects on Optoelectronic Properties of Monolayer Tungsten Disulfide. *Nanoscale* **2020**, *12*, 8344–8354.

(47) Tena, A.; Vazquez-Guilló, R.; Marcos-Fernández, A.; Hernández, A.; Mallavia, R. Polymeric Films Based on Blends of 6FDA-6FpDA Polyimide Plus Several Copolyfluorenes for CO₂ Separation. *RSC Adv.* **2015**, *5*, 41497–41505.


(48) Haddon, R. C. Chemistry of the Fullerenes: the Manifestation of Strain in a Class of Continuous Aromatic Molecules. *Science* **1993**, *261*, 1545–1550.


(49) McDonald, T. J.; Jones, M.; Engtrakul, C.; Ellingson, R. J.; Rumbles, G.; Heben, M. J. Near-Infrared Fourier Transform Photoluminescence Spectrometer with Tunable Excitation for the Study of Single-Walled Carbon Nanotubes. *Rev. Sci. Instrum.* **2006**, *77*, No. 053104.



JACS Au
AN OPEN ACCESS JOURNAL OF THE AMERICAN CHEMICAL SOCIETY

Editor-in-Chief
Prof. Christopher W. Jones
Georgia Institute of Technology, USA

Open for Submissions 

pubs.acs.org/jacsau  ACS Publications
Most Trusted. Most Cited. Most Read.